# Critical Role of Redox Mediator in Suppressing Charging Instabilities of Lithium−Oxygen Batteries

Zhuojian Liang and Yi-Chun Lu*

Electrochemical Energy and Interfaces Laboratory, Department of Mechanical and Automation Engineering, The Chinese University of Hong Kong, Hong Kong SAR 999077, China

Ⓢ Supporting Information

ABSTRACT: Redox mediators have been widely applied to reduce the charge overpotentials of lithium−oxygen (Li-O$_2$) batteries. Here, we reveal the critical role of redox mediator in suppressing the charging instability of Li-O$_2$ batteries. Using high temporal resolution online electrochemical mass spectrometry, we show that charging with redox mediators (using lithium bromide as a model system) significantly reduces parasitic gas evolution and improves oxygen recovery efficiency. Using redox mediator transforms the charge reactions from electrochemical pathways to chemical pathways, which unexpectedly bypasses the formation of highly reactive intermediates upon electro-oxidation of lithium peroxide (Li$_2$O$_2$). Such transformation reduces self-amplifying degradation reactions of electrode and electrolyte in Li-O$_2$ cells. We further show that the improved stability associated with the redox mediator is much more pronounced at higher charging rates, owing to fast charge-transfer kinetics of the redox mediator. Together, we show that employing redox mediator not only reduces the charge overpotential but also suppresses side reactions of Li-O$_2$ cells with improved charging rate. Our work demonstrates that transforming electro-oxidation of Li$_2$O$_2$ to chemical oxidation of Li$_2$O$_2$ is a promising strategy to simultaneously mitigate charging side reactions and achieve low overpotential for the Li-O$_2$ batteries.
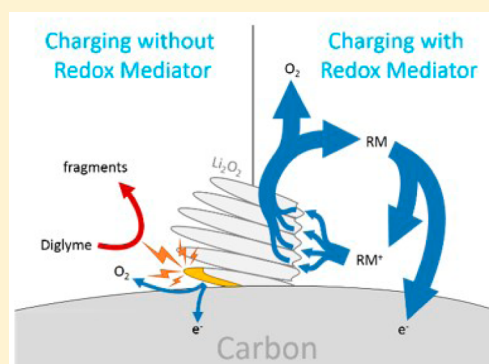
INTRODUCTION

Lithium−oxygen (Li-O$_2$) batteries have attracted intensive attention owing to their potential to provide gravimetric energy density 3−5 times that of conventional Li-ion batteries.[1−12] However, Li-O$_2$ technology suffers from poor cycle life (<100 cycles), low rate capability (<1 mA/cm^2), and poor round-trip efficiency (65−70%).[2−4,7−9,13,14] These challenges are intimately connected to technological barriers, including the sluggish discharge and charge reaction kinetics at the oxygen electrode,[15−18] chemical instabilities between reaction intermediates, electrolytes,[19−23] and carbon electrodes,[24−26] and sluggish transport kinetics.[27−33] Although ether-based electrolytes are relatively stable and yield Li$_2$O$_2$ as the main discharge product,[34] side reactions involving electrode and electrolyte are still widely observed and generate multiple side products such as LiOH, Li$_2$CO$_3$, and lithium acetate.[35−39] These side products cannot be fully removed without going to high cell voltages, which, however, triggers further electrolyte decomposition reactions.[2,24,25,35,40−42] Therefore, reducing charge overpotential[43−46] and side reactions[26] is an urgent task for developing nonaqueous Li-O$_2$ batteries.

Applying soluble redox mediator has been shown to effectively reduce discharge or charge overpotential of Li-O$_2$ batteries.[47−54] The charging mediator first gets oxidized at the electrode to form an oxidized species, which then chemically oxidizes the Li$_2$O$_2$ to evolve O$_2$.[47−54] For instance, lithium iodide (LiI),[49,54−57] tetrathiafulvalene (TTF),[47,58,59] phthalo-

cyanine (FePc),[60] 2,2,6,6-tetramethylpiperidinyloxyl (TEMPO),[50,61] 10-methylphenothiazine (MPT),[62] and tris[4-(diethylamino)phenyl]amine (TDPA)[63] were reported as charging redox mediators in Li-O$_2$ batteries. These redox mediators effectively decrease the charge potential from 4.3−4.5 V vs Li/Li$^+$ (all potentials hereinafter are referenced to Li/Li$^+$) to 3.3−3.6 V.

Despite the success in reducing reaction overpotential, there is a limited understanding of the effect of redox mediator on the reaction stability of Li-O$_2$ cells, which in fact is the most critical issue in Li-O$_2$ technology. In this work, we study the effect of redox mediator (using lithium bromide (LiBr) as a model system)[64,65] on the chemical stability of the Li-O$_2$ reactions via high temporal resolution online electrochemical mass spectrometry (OEMS). We believe that halides would form an excellent redox mediator set, given their tunability. We chose LiBr as the model system instead of LiI becuse (1) LiI is widely reported to promote side reactions involving LiOH,[66−68] and (2) the potentials of the two oxidation steps of LiBr are 3.48 and 4.0 V, slightly above the decomposition potentials of Li$_2$O$_2$ and Li$_2$CO$_3$. This allows us to investigate the mediation of both Li$_2$O$_2$ oxidation and Li$_2$CO$_3$ oxidation. We reveal that charging with the LiBr yields higher O$_2$ recovery rate and significantly reduces parasitic gas evolution. Interestingly, the reduced

overpotential and improved stability associated with LiBr are much more pronounced when charging at higher rates. Enhancement mechanisms responsible for the improved charging stability/efficiency with LiBr are discussed. Our work demonstrates that transforming electrochemical pathways to chemical pathways is a promising approach to simultaneously mitigate charging side reactions and achieve low overpotential for the Li-O$_2$ batteries.

■ MATERIALS AND METHODS

Electrolytes. Diethylene glycol dimethyl ether (diglyme, Sigma-Aldrich, anhydrous, 99.5%) was used as received, while lithium bis(trifluoromethane)sulfonimide (LiTFSI, Sigma-Aldrich, 99.95%) and LiBr (Sigma-Aldrich, 99.999%) were dried at 150 °C for 12 h in a glass oven (Büchi, Germany) under dynamic vacuum before being transferred to the glovebox. The transfers were done without exposing to the ambient atmosphere. All chemicals were stored in a glovebox (Etelux, China) where both H$_2$O and O$_2$ concentration are ≤1.0 ppm. For LiBr-free cells, 1 M LiTFSI in diglyme was used as the electrolyte. For LiBr-assisted cells, 10 mM LiBr−1 M LiTFSI in diglyme was used as the electrolyte. We note that 10 mM is sufficient to provide effective mediator function, and this concentration has been used in several studies.[47,50,54,58,59] Higher concentration of redox mediator is not used to avoid high capacity contribution from the redox mediator. The water content of all electrolytes was determined by Karl Fischer titration (TitroLine 7500 KF, SI Analytics) to be ≤25.0 ppm.

Electrode Fabrication. A slurry was prepared by dispersing 95 wt % Ketjenblack (EC-600JD, Akzo Nobel) and 5 wt% lithiated Nafion (Ion Power, USA) into isopropanol (Sigma-Aldrich, 99.7%), followed by ultrasonication with an ultrasonic probe (Shanghai Yanyong Ultrasonics, China) at 15W for 10 min. The slurry was then coated onto a piece of A4-size quartz fiber separator (QMA, Whatman) at a carbon loading of 0.4 ± 0.04 mg/cm^2. The electrodes were air-dried and punched (Φ16 mm) prior to drying in glass oven at 90 °C for 12 h. The transfers of dried electrodes were done without exposing to the ambient atmosphere.

Cell Assembly, Online Electrochemical Mass Spectrometer, and Electrochemical Characterization. Electrochemical cells were assembled in the glovebox by placing a piece of Ketjenblack cathode (described above, coated on quartz fiber separator) onto a Φ16 mm Li foil (MTI Co., China), followed by addition of 60 μL of electrolyte. The Li foil was treated with propylene carbonate (PC, Sigma-Aldrich, 99.7%). Above the cathode, a piece of Φ16 mm no. 400 SS316 mesh was added as a current collector, on which a Φ16 mm no. 100 SS316 mesh was placed to ensure good electrical contact. In tests where solid-state Li-conducting glass ceramic (LICGC, Φ19 mm, thickness 0.15 mm, Ohara, Japan) is used, a piece of Φ16 mm quartz fiber separator is placed on the Li anode, after which a piece of LICGC is added before stacking the Ketjenblack cathode and the two stainless steel meshes described above. A SS316 spring was employed to fix the electrodes, to avoid cracking of the LICGC, and to provide electrical contact with the top of the cell. In tests where the voltage of the Li counter electrode was measured, a third electric connection point was incorporated at the center of the anode side of the original cell, on which a piece of Φ3 mm Li was added as an independent reference electrode.

After assembly, the cell was connected to a pressure transducer (GB-3000HK, Gangbei Zhongtian Tech., China) and purged with O$_2$ (N5.0, HKO, Hong Kong) for 5 min to replace the Ar. The cell and the pressure transducer were filled with 1.2 bar of O$_2$ and allowed to rest for 20 min before discharge. Two SS316 tubes with ball valves were wielded on the top of the cell to allow the connection of the pressure transducer for O$_2$ consumption monitoring during discharge, or to allow continuous sampling of the evolved gas in the cell head space by the Ar carrier gas (N5.0, HKO, Hong Kong) and subsequent analysis in a mass spectrometer (QMS 200, Stanford Research Systems) during charge. The quantification of gas was calibrated by a standard gas mixture of O$_2$, CO$_2$, CO, H$_2$, and H$_2$O (5000 ppm each, balanced by Ar. Linde HKO, Hong Kong).

Galvanostatic discharge and charge tests and cyclic voltammetry tests were conducted using a VMP3 electrochemical testing station (Bio-logic). In these tests, assembled cells were rested for 20 min before cycling. Cells were purged continuously with diglyme-saturated 1.1 bar O$_2$ at 1 mL/min during both resting and cycling.
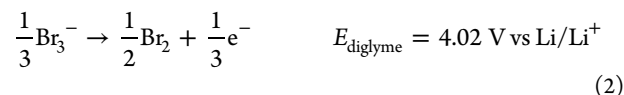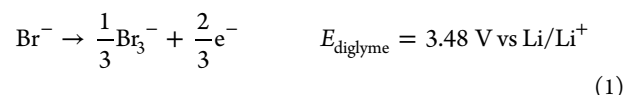
XRD Measurements. X-ray diffraction measurements were conducted on a Rigaku SmartLab diffractometer (Cu Kα radiation) at a scan rate of 0.6 degree/min. The samples were sealed on the sample holder by a Kapton tape in an Ar-filled glovebox.

NMR Measurements. NMR measurements were done using a Bruker 400 MHz NMR spectrometer. Discharged cathodes (with separators) were extracted with D$_2$O.

■ RESULTS AND DISCUSSION

Stability and Efficacy of LiBr as a Charging Mediator. We use lithium bromide as a model mediator. We first evaluate LiBr's stability in the presence of the O$_2$ gas. Lithium bromide displays two reversible redox reactions in the O$_2$-saturated electrolyte, as shown in the cyclic voltammograms (CVs) in Figure S1, which can be attributed to the following two redox reactions:[64]

$$Br^- \rightarrow \frac{1}{3}Br_3^- + \frac{2}{3}e^- \qquad E_{diglyme} = 3.48 \text{ V vs Li/Li}^+ \tag{1}$$

$$\frac{1}{3}Br_3^- \rightarrow \frac{1}{2}Br_2 + \frac{1}{3}e^- \qquad E_{diglyme} = 4.02 \text{ V vs Li/Li}^+ \tag{2}$$

The symmetric oxidation and reduction peaks shown in the CVs suggest that the Br$^-$/Br$_3^-$ (∼3.48 V) and Br$_3^-$/Br$_2$ (∼4.02 V) couples are electrochemically reversible and chemically stable in the presence of the O$_2$ gas. We here provide the redox potential based on the CVs conducted in diglyme (Figure S1), and we note that the equilibrium voltages for reactions 1 and 2 are solvent dependent, since the solvent-dependent solvation energy of the bromide and tribromide ions will influence the reversible potential. The stability of the Br-containing species (e.g., Br$^-$/Br$_3^-$/Br$_2$) with the diglyme was further confirmed using Fourier transform infrared spectroscopy (FTIR) and electrospray ionization mass spectrometry (ESI-MS), as shown in Figures S2 and S3.
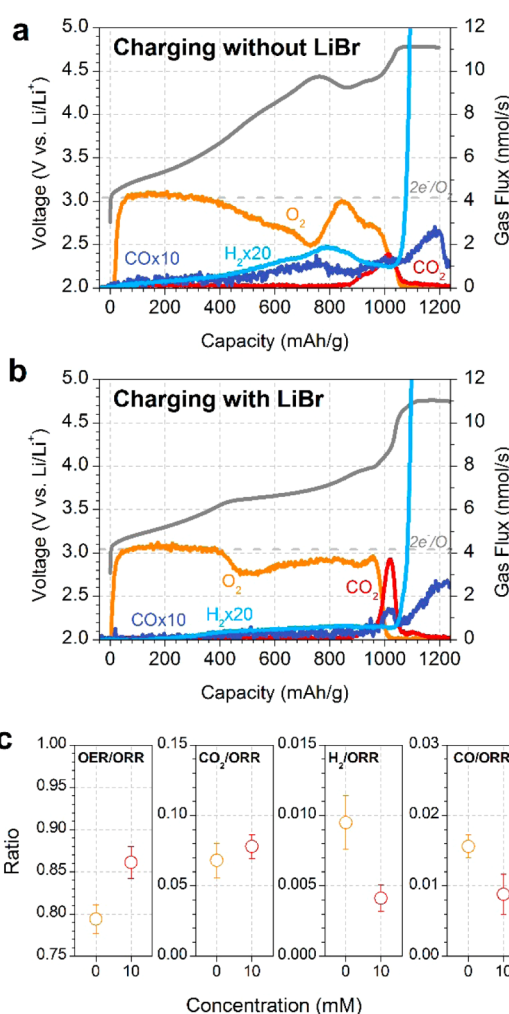
Next, we evaluate the efficacy of LiBr as a charging mediator of Li-O$_2$ batteries. Figure 1 shows the galvanostatic voltage profiles of Li-O$_2$ cells with and without LiBr at 500 mA/g, 1000 mA/g, and 2000 mA/g (normalized to the mass of carbon, the same hereafter). The charging potential was significantly lowered by the LiBr at all rates, while the discharge potentials were unaffected. We quantified the O$_2$ pressure reduction during discharge (i.e., oxygen reduction reaction, ORR) for cells with and without LiBr and found a 2e$^-$/O$_2$ process for both cells (Figure S4), which agrees well with the Li$_2$O$_2$ phase identified in the XRD spectra of the discharged electrodes for both cells (Figure S5). Upon charging, the charging voltage of the cells without LiBr (LiBr-free cells) overlapped with the cells with LiBr (LiBr-assisted cells) at voltages below 3.5 V, after which the charging voltage of the LiBr-free cells keep increasing with a similar slope until reaching voltage higher than 4.3 V. In contrast, the charging voltage of the LiBr-assisted cells started to deviate from the LiBr-free cells from 3.5 V onward, with a much reduced slope. This indicates that the LiBr mediator is activated, i.e., gets oxidized to form Br$_3^-$, which then chemically oxidizes the discharge products of the Li-O$_2$ cells.[69] The transition voltage is consistent with the reaction potential of
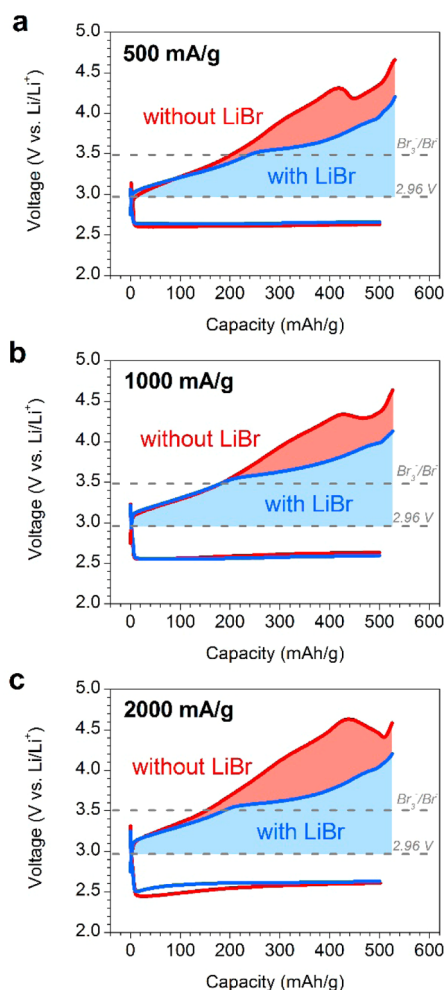
Figure 1. Galvanostatic discharge/charge profiles of Li-O_2 cells with and without 10 mM LiBr at (a) 500, (b) 1000, and (c) 2000 mA/g. The rates are equivalent to 0.2, 0.4, and 0.8 mA/cm^2, respectively.

Figure 2. Voltage and gas evolution profiles during charging (a) without and (b) with 10 mM LiBr after discharge to 1000 mAh/g at 1000 mA/g. (c) Statistics based on at least three replications.

reaction 1 observed in the CV test (3.48 V, Figure S1). In addition, the voltage gap between cells with and without LiBr increases with charging rates and reaches a 780 mV voltage reduction at a high charging rate of 2000 mA/g (0.8 mA/cm^2). This suggests that the charge-transfer kinetics of the Br^-/Br_3^- couple is faster than the charge-transfer kinetics of Li_2O_2 oxidation (and possibly LiO_2 oxidation simultaneously[70−74]) on the carbon electrodes. The voltage profiles of the mediated Li-O_2 charging increase slowly with capacity (instead of a complete flat plateau). This is consistent with many of other reported redox mediators, which can be attributed to the oxidation of carbonates (will be discussed below) and/or the depletion of rechargeable products.[50]

The efficacy of the LiBr as a redox mediator to evolve oxygen is further supported by the online monitoring of the gas evolution upon charging using an OEMS system. Figure 2 shows the cell voltage and online gas evolution profile during charging of cells with and without LiBr after discharge to 1000 mAh/g. The major gas evolved in both cells was O_2. The dominating reaction in the LiBr-free cells and LiBr-assisted cells before 3.5 V was consistent with the electrochemical oxidation of Li_2O_2:

$$Li_2O_2 \rightarrow 2Li^+ + O_2 + 2e^- \tag{3}$$

For the LiBr-assisted cells between 3.5 and 3.9 V, the dominating electrochemical reaction is the oxidation of Br^- to from Br_3^-, which then chemically oxidizes Li_2O_2, yielding

$$Li_2O_2 + Br_3^- \rightarrow 2Li^+ + O_2 + 3Br^- \tag{4}$$
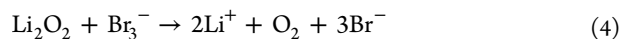
The capacity of the redox mediator is quantified to be about 2% of the capacity of oxygen reduction reaction (Supporting Information). The absence of noticeable shuttling of the Br_3^- mediator indicates that Br_3^- is effectively converted back to Br^- by reacting with the Li_2O_2. The stability of the lithium anode in the presence of LiBr is investigated. Figure S6 shows that the overpotential of the lithium anode is small (±2 mV) and stable over cycling with and without LiBr. Oxygen recovery efficiency, which is defined as the ratio of the amount of O_2 evolved upon charge to the amount of O_2 consumed during discharge (OER/ORR), is commonly used to describe the overall stability of the system.[75−78] We calculate the O_2 recovery efficiency based on the integrated amount of O_2 evolution during charge and the O_2 uptake monitored by pressure transducer during discharge. Ratios of CO_2/ORR, H_2/ORR, and CO/ORR are also quantified with the same method. These ratios are shown in Figure 2c with error bars calculated with at least three replications. The results show that the LiBr-assisted cells exhibit higher OER/ORR ratio compared to the LiBr-free cells. This

agrees with the rise of oxygen recovery efficiency from 0.86 to 0.92 observed by Meini et al. using LiI,[77] and from 0.65 to 0.74 observed by Kundu et al. using TDPA.[63] More importantly, the LiBr-assisted cells show lower H_2/ORR and lower CO/ORR compared to the LiBr-free cells. We note that improved stability is also observed when using LiI, however, with smaller degree of improvement compared to using LiBr (Figure S7). This may be related to the formation of side products like LiOH promoted by the use of LiI.[66−68] In short, we show that applying LiBr improves the oxygen recovery efficiency and reduces parasitic H_2 and CO evolutions. This demonstrates that LiBr not only reduces the charging overpotential but also effectively reduces the charging side reactions.

How Does LiBr Reduce Charging Side Reactions? Here we examine the origin of the higher O_2 recovery efficiency and reduced parasitic gas evolutions when charging with LiBr.

Electrochemical Charging Processes (LiBr-Free). For the LiBr-free cells (Figure 2a), oxygen was evolved at the ideal rate of $2e^-/O_2$ at the beginning, followed by a minor declination, and then an accelerated drop starting from 400 mAh/g (ca. the first 1/3 of the charge capacity), accompanied by H_2 and CO evolutions (Figure 2a). We note that the MS signal of $m/z = 28$ is not from ethylene (C_2H_4) since no signals at $m/z = 27$ (25% for C_2H_4) nor $m/z = 26$ (24% for C_2H_4) were identified together with $m/z = 28$ (Figure S8). Therefore, we assign the signal at $m/z = 28$ to carbon monoxide (CO). At a capacity around 750 mAh/g (ca. at 2/3 of the charge capacity), the O_2 evolution rate rose back, which synchronizes with the decreases in voltage, H_2, and CO evolution. These features indicate that side reactions associated with H_2 and CO evolutions first appeared and then went down during this period.[79] We note that such a dip observed in the O_2 evolution profile is not electrode-specific because it was widely observed by many research groups during charging using carbon[20,76,78,80−82] and a number of non-carbon cathodes,[1,83,84] nor is it electrolyte-specific because it was observed in dimethyl sulfoxide (DMSO),[1,76] ethereal,[20,63,76,80−83] acetonitrile,[76] N-methylpyr-rolidone (NMP),[76] and silane-based[76] electrolytes. We believe that it is an intrinsic instability associated with electrochemical oxidation of Li_2O_2 that occurs at the Li_2O_2−electrolyte interface.

We carried out detailed OEMS analysis to investigate the origin of the parasitic gas evolution. There are two possible sources of H_2/CO: (1) it can evolve directly from the cathode side from diglyme decomposition and/or (2) from side reactions between the lithium anode and the dissolved cathode decomposition products (e.g., protic species) migrating from the cathode to the anode. To distinguish these two sources, we employed a solid-state Li-conducting glass ceramic (LICGC) between the cathode and the separator to (1) reduce gas signals from the anode and (2) remove interactions between the cathode and the anode, i.e., to prevent dissolved reactive species (e.g., protic species) migrating from the cathode to the anode and reacting with lithium to evolve H_2 (photographs of the OEMS cells in Figure S9 shows no liquid communication between the cathode and the anode when using LICGC and 60 μL of electrolyte on both sides). With the LICGC, the LiBr-free cells (Figure 3a) showed similar H_2 and CO evolution with slightly lower rates and narrower H_2 peak shape compared to the LiBr-free cells without LICGC (Figure 2a). This suggests that the majority of H_2 and CO in this range evolves directly from the cathode with the minority resulted from the anode. Based on this observation, we propose that the formation of H_2
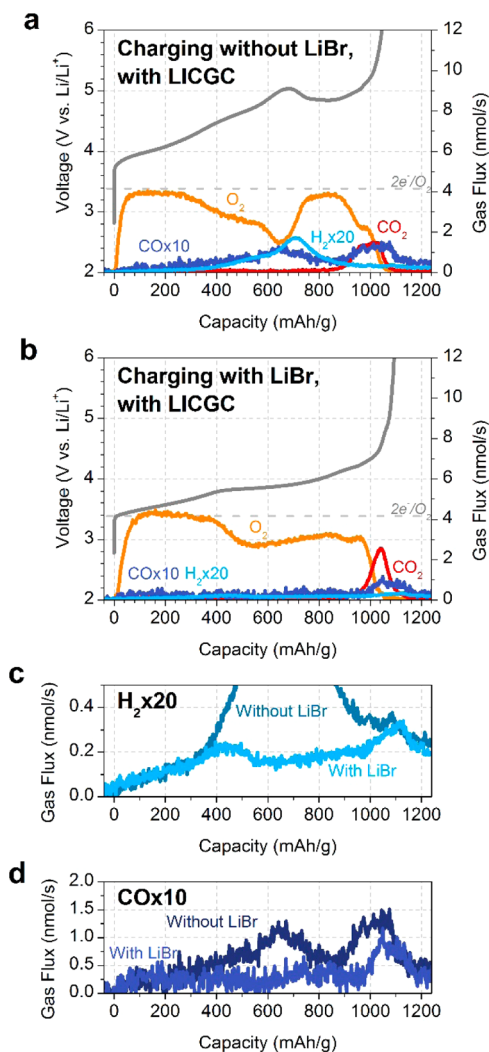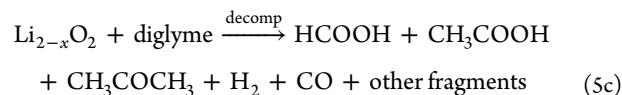

Figure 3. Voltage and gas evolution profiles during charging with a piece of LICGC inserted between the carbon cathode and the Li anode in cells (a) without and (b) with 10 mM LiBr. The H_2 and CO evolution profiles are compared in panels (c) and (d).

and CO with reduced O_2 evolution rate in the LiBr-free cells can be attributed to the degradation of diglyme triggered by $Li_{2-x}O_2$ phase[70,74,85−90] to form fragments:[91]

$$Li_2O_2 \rightarrow xLi^+ + Li_{2-x}O_2 + xe^- \tag{5a}$$

$$Li_{2-x}O_2 + diglyme \rightarrow fragments \tag{5b}$$
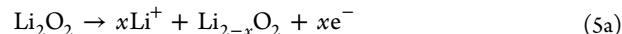
These reactions will lead to reduction in the O_2 evolution rate,[92] and the fragments can be further decomposed into carbonates[35,93] or protic species.[77,94] This is supported by the ^{1}H NMR spectrum of the cycled cathode and electrolyte (Figure 4), showing evidence of formic acid, acetic acid, and acetone.[50,63] Based on the evidence of OEMS and ^{1}H NMR, a possible expression of the side reaction could be

$$Li_{2-x}O_2 + diglyme \xrightarrow{decomp} HCOOH + CH_3COOH$$
$$+ CH_3COCH_3 + H_2 + CO + other\ fragments \tag{5c}$$

In fact, the formation of the highly reactive intermediate species during Li_2O_2 oxidation (e.g., $Li_{2-x}O_2$) has been suggested in the literature,[40,85] and our OEMS and NMR results provide strong evidence to reveal charging instabilities that occur during
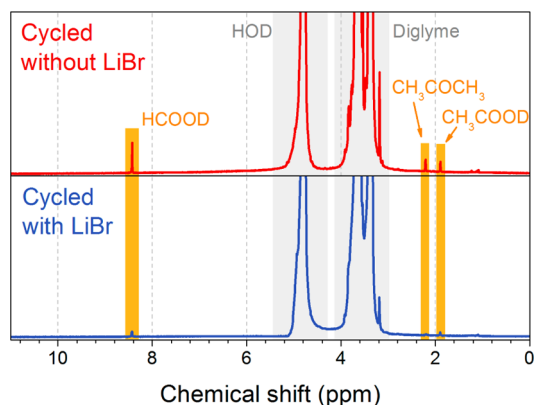
Figure 4. ^1H NMR spectra of the cathode and electrolyte after five cycles of galvanostatic cycling (at 1000 mA/g to 1000 mAh/g) with and without 10 mM LiBr in the electrolyte. The spectra were calibrated and normalized to HOD at 4.79 ppm. The peaks at 8.43, 2.21, and 1.89 ppm are assigned to formate, acetone, and acetate, respectively.

electrochemical oxidation of Li_2O_2. We believe that its Li deficiency makes it an aggressive oxidant toward the diglyme electrolyte molecules. This is supported by a computational study suggesting that nucleophilic attack on 1,2-dimethoxy-ethane (DME, shares similar ethereal functional group with diglyme) by superoxide termination is kinetically faster than peroxide termination, especially in the presence of a charging electric field.[91] Those researchers also found that DME is decomposed in an H-abstraction pathway with OH^- ion and DME fragments as the decomposition products.

As Li_2O_2 was gradually removed, O_2 evolution was followed by CO_2 evolution from the decomposition of carbonates (Figures 2a and 3a).[41,95] The CO_2 evolution was accompanied by a rise in the CO signal, which is observed in the LiBr-free cells regardless of LICGC (Figures 2a and 3a). This can be attributed to the attack on the carbon electrode by radicals[95,96] generated from carbonate decomposition by

$$4Li_2CO_3 \rightarrow 6Li^+ + 4CO_2 + 2LiO_2 + 6e^- \qquad (6a)$$
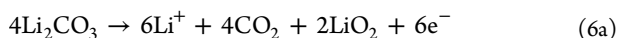
whose reversible potential can be estimated to be between 3.85 and 4.09 V (Supporting Information). This route is consistent with Yang et al., showing the formation of O_2^- upon oxidation of Li_2CO_3.[96] Subsequently, O_2^- was shown to attack carbon support:[24,95]

$$2LiO_2 + 2C \rightarrow CO + Li_2CO_3 \qquad (6b)$$
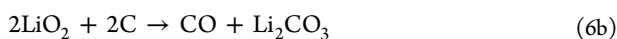
This will give an overall reaction:

$$3Li_2CO_3 + 2C \rightarrow 6Li^+ + 4CO_2 + CO + 6e^- \qquad (6c)$$

Finally, after the end of carbonates decomposition, diglyme electrolyte decomposition dominated the reaction, as indicated by the voltage plateau and the significant rise in H_2 and CO evolutions (Figure 2a).

In short, these observations suggest that *electrochemical oxidation of Li_2O_2* generates reactive intermediate species that cause electrolyte decomposition to evolve H_2 and CO. Strategies that avoid/bypass the electrochemical oxidation of Li_2O_2 could potentially mitigate these side reactions.
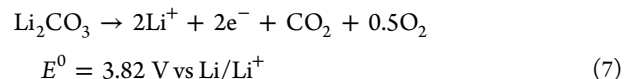
Chemical Charging Processes (LiBr-Assisted). Charging with LiBr not only reduces the amount of H_2 and CO evolution but also changes their patterns. When charging with LiBr before reaching 3.5 V (Figure 2b), both voltage and gas evolution

profiles are the same as those for the cell without LiBr (i.e., in the first 400 mAh/g). After the onset of LiBr oxidation (reaction 1), the O_2 evolution continues deviating from $2e^-/O_2$ but soon rose back at 500 mAh/g, *without* obvious increase in H_2 and CO evolution, which is in strong contrast to that observed in cells without LiBr (Figure 2a). The deviation of the O_2 evolution from $2e^-/O_2$ can be attributed to (1) the activation of the LiBr mediator[63] and/or (2) parasitic reactions resulting from electro-oxidation of Li_2O_2 that consumes O_2 and/or evolves H_2/CO (e.g., reactions 5a,b). This is related to the fact that the electro-oxidation of Li_2O_2 may still take place in the presence of LiBr, but at a much lower rate compared to the LiBr-free cells, since the majority of the current will be carried by the Br^-/Br_3^- redox couple. To understand the source of the minor H_2 and CO evolution observed in the LiBr cells, we employed LICGC between the cathode and the separator for LiBr-assisted cells (Figure 3b). Surprisingly, the majority of the H_2 and CO evolution can be removed (Figure 3c,d). This is in strong contrast to the observation with LiBr-free cells, where the H_2 and CO evolutions are still very prominent with LICGC (Figure 3a). This demonstrates that (1) the sources of H_2 and CO evolutions observed in the LiBr-assisted cells in Figure 2b are mainly from the lithium negative electrode, and (2) H_2/CO evolutions from the positive electrode are substantially suppressed by LiBr upon its activation (Figure 3c,d). Since charging with LiBr proceeds mainly with chemical oxidation of Li_2O_2 by Br_3^- (reaction 4) instead of electrochemically oxidizing Li_2O_2 (reaction 5a), we hypothesize that it bypasses the formation of the highly reactive $Li_{2-x}O_2$ species,[40,85] which could then avoid diglyme decomposition to evolve H_2 and CO (e.g., reactions 5a,b). This hypothesis is further supported by the ^1H NMR spectrum of the cathode and electrolyte cycled with LiBr (Figure 4), which shows relatively lower concentration of formic acid, acetic acid, and acetone as compared to those of the LiBr-free cell. Similar mitigation of fragment formation has been observed by Kundu et al. after cycling a cell with TDPA in TEGDME-based electrolyte,[63] and by Qiao et al. after charging with TTF in DMSO-based electrolyte.[59]
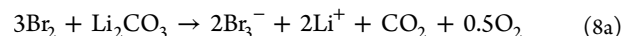
As the voltage further increased to 3.90 V (Figure 2b) CO_2 began to evolve accompanied by an increase in CO evolution. We believe that the oxidation of Li_2CO_3 is mediated by the mediator, as evidenced by the following findings: (1) the onset oxidation potential of Br_3^- to form Br_2 is around 3.9 V (Figure S1), and (2) the onset voltage of CO_2 evolution in the presence of LiBr is much lower than that of the LiBr-free cells (4.35 V). The mediator-assisted Li_2CO_3 oxidation could occur with or without generation of CO. First, Br_3^- can be oxidized to Br_2, which can oxidize Li_2CO_3 to evolve CO_2 and O_2 as follows (see eq 2):

$$2Br_3^- \rightarrow 3Br_2 + 2e^- \qquad E_{diglyme} = 4.02 \text{ V vs Li/Li}^+$$

and since

$$Li_2CO_3 \rightarrow 2Li^+ + 2e^- + CO_2 + 0.5O_2$$
$$E^0 = 3.82 \text{ V vs Li/Li}^+ \qquad (7)$$

thus Br_2 can oxidize Li_2CO_3 to yield:

$$3Br_2 + Li_2CO_3 \rightarrow 2Br_3^- + 2Li^+ + CO_2 + 0.5O_2 \qquad (8a)$$

Alternatively, the oxidation of Li_2CO_3 could generate LiO_2 radical[96] as described in reaction 6a, which can be combined with reaction 2 to yield
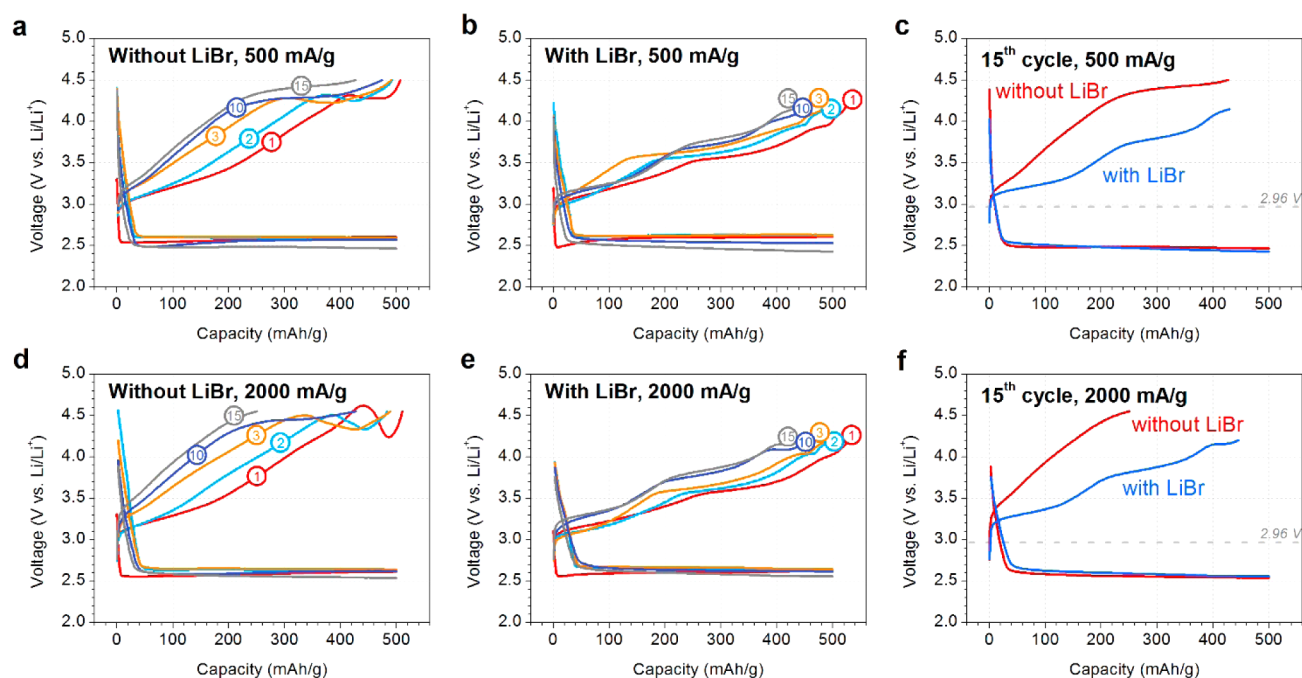
Figure 5. Selected cycles of cells cycled without and with 10 mM LiBr at (a,b) 500 and (c,d) 2000 mA/g charging rate, with a discharge capacity of 500 mAh/g and discharge rate of 1000 mA/g. The 15th cycles are compared in (c) and (f).

$$9Br_2 + 4Li_2CO_3 \rightarrow 6Li^+ + 4CO_2 + 2LiO_2 + 6Br_3^-$$
$$(8b)$$
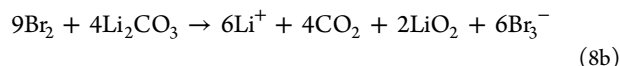
In addition, O_2^- was shown[24,95] to attack carbon support (see reaction 6b). Combining reactions 8b and 6b will give

$$9Br_2 + 3Li_2CO_3 + 2C \rightarrow 6Br_3^- + 6Li^+ + 4CO_2 + CO$$
$$(8c)$$

Finally, as the charge capacity exceeds the discharge capacity, the decomposition of diglyme dominates the reaction and leads to a rise in the H_2 and CO evolutions (Figure 2b;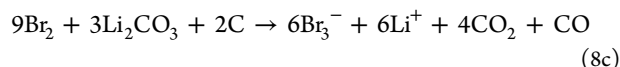 also see Figure 7, below), which is similar to that observed in LiBr-free cells (Figure 2a). We note that the charge voltage of cells with LICGC (Figure 3, regardless of LiBr) drastically increases at the end of charge without further increase in gas evolution. This is in strong contrast to the observation with cells without LICGC (Figure 2, regardless of LiBr), where the voltage was plateaued with significant increase in H_2 and CO evolutions. This can be attributed to that the LICGC blocked the shuttle current from the electrolyte decomposition fragments that diffuse between the cathode and the anode.

The reduced charging side reactions resulted from LiBr improves the cycling stability of the Li-O_2 batteries. Figure 5 shows the galvanostatic voltage profiles of cells with and without LiBr at charging rates of 500 mA/g and 2000 mA/g. The charging voltages of LiBr-free cells grow substantially with cycling (Figure 5a,d), which is consistent with typical cycling profiles of Li-O_2 batteries with carbon cathode.[2,47,97] On the contrary, the cycling profiles of the LiBr-assisted cells are much more stable than the LiBr-free cells. Figure 5c,f compares the voltage profiles of the Li-O_2 cells with and without LiBr at 15th cycles. Comparing with the profiles in the first cycle (Figure 1), the reduction in charge voltage associated with LiBr is much more pronounced at the 15th cycle. In addition, cycling with LiBr also benefits the nonmediated region (ca. below 3.5 V) as shown in the reduced charging voltage in the LiBr-assisted cells at the 15th cycle, which can be attributed to a reduction in

accumulated side-products.[24] A comparison of the gas evolution during a full charge of the fifth cycle is shown in Figure S11. Comparing with the OEMS results on the first charge, the large amount of CO_2 evolution at the fifth cycle in both cells suggests the accumulation of carbonates upon cycling. However, the LiBr-free cell showed substantially increased H_2 evolution at fifth cycle compared to the first cycle (Figure 2a). This indicates that the stability of the LiBr-free cell has been severely impaired by self-amplifying parasitic reactions.[2,24,25,35,40−42] In contrast, the LiBr-assisted cell showed similar amount of H_2 evolution between the first and the fifth cycles, which suggests that the enhanced stability associated with LiBr is preserved upon cycling. Overall, these observations suggest that reducing charging side reaction by LiBr greatly improve the cycling stability of Li-O_2 cells.

We summarize observations and hypothesis in Figure 6 to illustrate the differences in reaction pathways between electrochemical charging and chemical charging by LiBr. Our study suggests that when charging without LiBr, electrochemical oxidation of Li_2O_2 generates reactive intermediates that trigger degradation reactions of electrolyte and electrode.[34,76,81,98,99] On the contrary, when charging with LiBr, Li_2O_2 is chemically oxidized by Br_3^- instead of undergoing electrochemical delithiation, which may bypass the formation of reactive intermediate species, e.g., $Li_{2-x}O_2$,[40,85,100] leading to reduced side reactions upon charging Li-O_2 batteries. We note that LiBr serves as a model system here to illustrate the role of redox mediator in suppressing charging side reactions, rather than as a final solution for Li-O_2 batteries since its reversible potential is higher than those of LiI[49,54−57] and TDPA.[63]

Effect of Charging Rate on the Competition of Charging Pathways. We further investigate the influence of charging rate on the effectiveness of LiBr mediator in the Li-O_2 cells. Gas evolution was monitored at different current rates for LiBr-assisted cells as shown in Figure 7. Surprisingly, the OER efficiency of the LiBr-assisted cells is increased from 500 mA/g
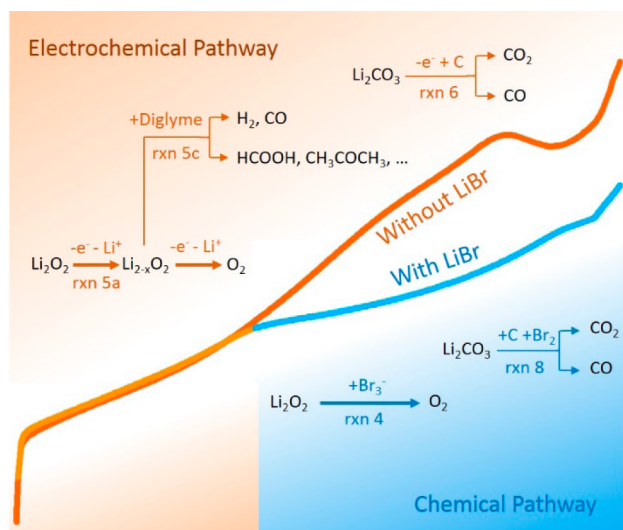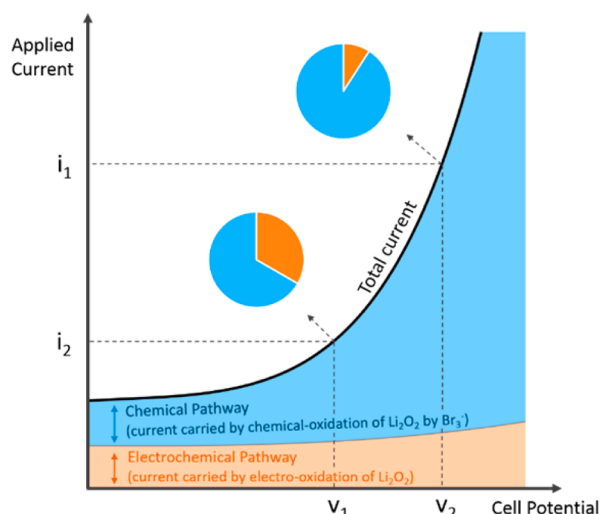
Figure 6. Schematic illustration of the different reaction (rxn) mechanisms when charged with and without LiBr.

(OER/ORR = 0.61 ± 0.02) to 2000 mA/g (OER/ORR = 0.98 ± 0.05). The rate-dependent enhancement of the O_2 evolution rate can be categorized into two stages, i.e., before and after 3.5 V (the activation of LiBr). First, before 3.5 V (prior to the activation of LiBr), the O_2 evolution rates are similar in the LiBr-free and LiBr-assisted cells at the same charge rate, as shown in Figure S12. Interestingly, the O_2 evolution rate is improved as the charge rate increases for *both* LiBr-free and LiBr-assisted cells. This shows that charging Li-O_2 cells at higher rate improves the O_2 evolution rate, regardless of LiBr. This could be related to the rate-dependent charging pathways of Li_2O_2 and requires further studies. Second, after 3.5 V (after the activation of LiBr), the O_2 evolution rates are much higher for the LiBr-assisted cell than the LiBr-free cell at the same charge rate, as shown in Figure S12. The rate-dependent enhancement in O_2 evolution rate is more pronounced for the LiBr-assisted cell than the LiBr-free cell after LiBr is activated. For instance, we quantify the O_2 evolution efficiency after 3.5 V for both cells (calculation method is included in Supporting Information). For the LiBr-assisted cells, the O_2 evolution efficiency after 3.5 V is 0.52 at 500 mA/g, 0.77 at 1000 mA/g, and 0.97 at 2000 mA/g; for the LiBr-free cells, the O_2 evolution efficiency after 3.5 V is 0.48 at 500 mA/g, 0.68 at 1000 mA/g, and 0.84 at 2000 mA/g. This observation supports that the improvement in O_2 evolution rate associated with LiBr is more pronounced at higher charging rate. Considering the high oxidation kinetics of the Br^-/Br_3^- couple[101,102] and the sluggish electro-oxidation kinetics of Li_2O_2,[2,103] when the applied charging rate increases, the percentage of the current associated with the oxidation of Br^- increases compared with the percentage of the current associated with electro-oxidation of Li_2O_2, as illustrated in Figure 8. This is consistent with the fact that the Br^-/Br_3^- exhibits lower Tafel slope (60 mV/dec)[101] compared to the electro-oxidation of Li_2O_2 (250−382 mV/dec).[2,103] In other words, it is advantageous to charge a LiBr-assisted Li-O_2 cell at high rates to promote the chemical pathways by the mediators. This is supported by the fact that the improvement in the cycling stability associated with LiBr at 2000 mA/g is more pronounced than the improvement observed at 500 mA/g (Figure 5c,f). To further improve the cycling life, combining effective redox mediators for both
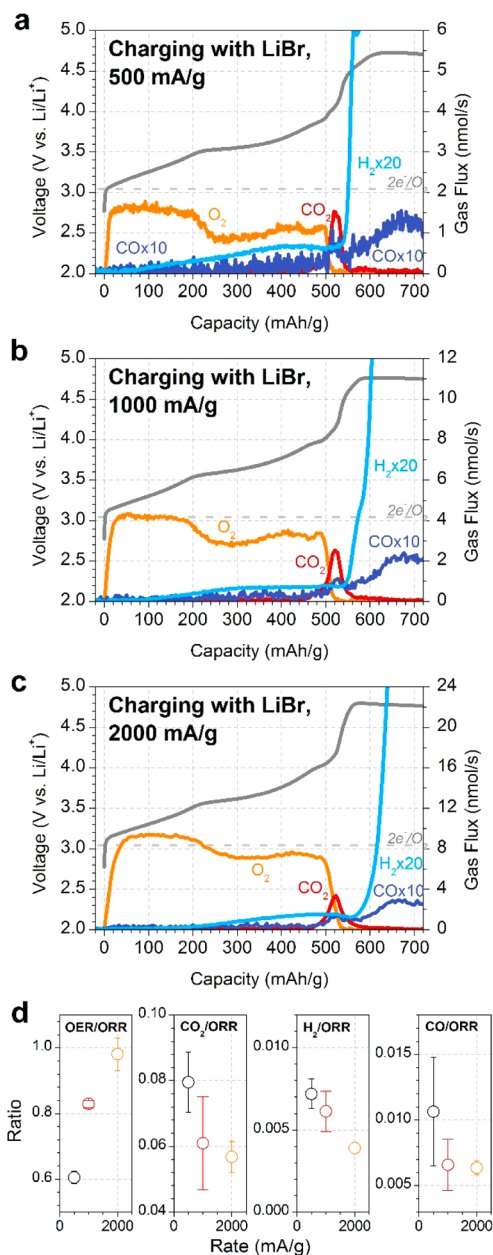
Figure 7. Voltage and gas evolution profiles during charging with 10 mM LiBr at (a) 500, (b) 1000, and (c) 2000 mA/g after discharge to 500 mAh/g at 1000 mA/g. Panel (d) shows statistics based on at least three replications. A figure without magnification of H_2 is shown in Figure S10.

discharge and charge reactions[54,60] will offer promising opportunities to mitigate chemical instabilities during both discharge and charge reactions of the Li-O_2 batteries. We note that potential additional parasitic reactions and products formed during charging through a chemical process via redox mediator should be considered. For instance, LiI was shown to promote the formation of LiOH.[66−68] In our study, no additional parasitic product can be identified for the LiBr-assisted cells using OEMS, XRD, NMR, FTIR, and ESI-MS. Further investigations using other spectroscopic and microscopic techniques are ongoing.

Figure 8. Schematic illustration of the effect of charging rate on the competition of charging pathways.

CONCLUSION

In summary, we reveal the critical role of redox mediator in suppressing the charging instabilities of Li-O$_2$ batteries. We showed that charging with redox mediator (e.g., LiBr) simultaneously reduces charging overpotential and suppresses charging parasitic reactions. LiBr exhibits two oxidation steps that align with the oxidation potentials of Li$_2$O$_2$ and Li$_2$CO$_3$ and was shown to be effective in oxidizing Li$_2$O$_2$ and Li$_2$CO$_3$ formed in the Li-O$_2$ batteries. We revealed the prominent effect of a chemical charging pathway in suppressing side reactions. We further showed that charging stability is improved at higher charging rates and that the mediator's effectiveness in suppressing side reactions is much more pronounced at high charging rates owing to fast charge-transfer kinetics of the redox mediator. Our work demonstrates that transforming electro-oxidation of Li$_2$O$_2$ to chemical oxidation of Li$_2$O$_2$ is a promising strategy to simultaneously mitigate reaction instabilities and achieve low overpotentials for Li-O$_2$ batteries.

ASSOCIATED CONTENT

Ⓢ Supporting Information

The Supporting Information is available free of charge on the ACS Publications website at DOI: 10.1021/jacs.6b01821.

> Figures S1−S12, showing cyclic voltammograms of LiBr; FTIR and ESI-MS spectra of electrolytes; OEMS results of O$_2$ consumption during discharge; XRD patterns of positive electrodes after discharge; voltage profiles of the lithium anode upon cycling; OEMS results of gas evolution during charging with LiI and of ethane-related signals during charging; photos of OEMS cell with LICGC; voltage and gas evolution profiles (without H$_2$ magnification) of charging at different rates; OEMS results of O$_2$ consumption and gas evolution at the fifth cycle; and voltage and gas evolution profiles of charging at different rates without LiBr; and discussions on capacity contribution from LiBr and estimation of the reversible potential of reaction 6a (PDF)

AUTHOR INFORMATION

Corresponding Author

*yichunlu@mae.cuhk.edu.hk

REFERENCES

(1) Luntz, A. C.; McCloskey, B. D. *Chem. Rev.* **2014**, *114*, 11721−50.
(2) Lu, Y.-C.; Gallant, B. M.; Kwabi, D. G.; Harding, J. R.; Mitchell, R. R.; Whittingham, M. S.; Shao-Horn, Y. *Energy Environ. Sci.* **2013**, *6*, 750−768.
(3) Bruce, P. G.; Freunberger, S. A.; Hardwick, L. J.; Tarascon, J. M. *Nat. Mater.* **2012**, *11*, 19−29.
(4) Black, R.; Adams, B.; Nazar, L. F. *Adv. Energy Mater.* **2012**, *2*, 801−815.
(5) Abraham, K. M.; Jiang, Z. *J. Electrochem. Soc.* **1996**, *143*, 1−5.
(6) Li, F.; Wu, S.; Li, D.; Zhang, T.; He, P.; Yamada, A.; Zhou, H. *Nat. Commun.* **2015**, *6*, 7843.
(7) Girishkumar, G.; McCloskey, B.; Luntz, A. C.; Swanson, S.; Wilcke, W. *J. Phys. Chem. Lett.* **2010**, *1*, 2193−2203.
(8) Shao, Y. Y.; Park, S.; Xiao, J.; Zhang, J. G.; Wang, Y.; Liu, J. *ACS Catal.* **2012**, *2*, 844−857.
(9) Christensen, J.; Albertus, P.; Sanchez-Carrera, R. S.; Lohmann, T.; Kozinsky, B.; Liedtke, R.; Ahmed, J.; Kojic, A. *J. Electrochem. Soc.* **2012**, *159*, R1−R30.
(10) Shao, Y.; Ding, F.; Xiao, J.; Zhang, J.; Xu, W.; Park, S.; Zhang, J.-G.; Wang, Y.; Liu, J. *Adv. Funct. Mater.* **2013**, *23*, 987−1004.
(11) McCloskey, B. D.; Burke, C. M.; Nichols, J. E.; Renfrew, S. E. *Chem. Commun.* **2015**, *51*, 12701−15.
(12) Lu, J.; Lau, K. C.; Sun, Y.-K.; Curtiss, L. A.; Amine, K. *J. Electrochem. Soc.* **2015**, *162*, A2439−A2446.
(13) Xia, C.; Waletzko, M.; Peppler, K.; Janek, J. *J. Phys. Chem. C* **2013**, *117*, 19897−19904.
(14) McCloskey, B. D.; Scheffler, R.; Speidel, A.; Girishkumar, G.; Luntz, A. C. *J. Phys. Chem. C* **2012**, *116*, 23897−23905.
(15) Lu, Y.-C.; Gasteiger, H. A.; Shao-Horn, Y. *J. Am. Chem. Soc.* **2011**, *133*, 19048−19051.
(16) Lu, Y.-C.; Shao-Horn, Y. *J. Phys. Chem. Lett.* **2013**, *4*, 93−99.
(17) Safari, M.; Adams, B. D.; Nazar, L. F. *J. Phys. Chem. Lett.* **2014**, *5*, 3486−91.
(18) Wijaya, O.; Hartmann, P.; Younesi, R.; Markovits, I. I. E.; Rinaldi, A.; Janek, J.; Yazami, R. *J. Mater. Chem. A* **2015**, *3*, 19061−19067.
(19) Aurbach, D.; Daroux, M. L.; Faguy, P.; Yeager, E. *J. Electroanal. Chem. Interfacial Electrochem.* **1991**, *297*, 225−244.
(20) McCloskey, B. D.; Bethune, D. S.; Shelby, R. M.; Girishkumar, G.; Luntz, A. C. *J. Phys. Chem. Lett.* **2011**, *2*, 1161−1166.
(21) Hyoung Oh, S.; Yim, T.; Pomerantseva, E.; Nazar, L. F. *Electrochem. Solid-State Lett.* **2011**, *14*, A185.
(22) Khetan, A.; Luntz, A.; Viswanathan, V. *J. Phys. Chem. Lett.* **2015**, *6*, 1254−9.
(23) Xu, W.; Hu, J.; Engelhard, M. H.; Towne, S. A.; Hardy, J. S.; Xiao, J.; Feng, J.; Hu, M. Y.; Zhang, J.; Ding, F.; Gross, M. E.; Zhang, J.-G. *J. Power Sources* **2012**, *215*, 240−247.
(24) McCloskey, B. D.; Speidel, A.; Scheffler, R.; Miller, D. C.; Viswanathan, V.; Hummelshøj, J. S.; Nørskov, J. K.; Luntz, A. C. *J. Phys. Chem. Lett.* **2012**, *3*, 997−1001.
(25) Ottakam Thotiyl, M. M.; Freunberger, S. A.; Peng, Z.; Bruce, P. G. *J. Am. Chem. Soc.* **2013**, *135*, 494−500.
(26) Lu, J.; Lei, Y.; Lau, K. C.; Luo, X.; Du, P.; Wen, J.; Assary, R. S.; Das, U.; Miller, D. J.; Elam, J. W.; Albishri, H. M.; El-Hady, D. A.; Sun, Y. K.; Curtiss, L. A.; Amine, K. *Nat. Commun.* **2013**, *4*, 2383.

(27) Radin, M. D.; Rodriguez, J. F.; Tian, F.; Siegel, D. J. *J. Am. Chem. Soc.* **2012**, *134*, 1093−1103.

(28) Gerbig, O.; Merkle, R.; Maier, J. *Adv. Mater.* **2013**, *25*, 3129−3133.

(29) Dunst, A.; Epp, V.; Hanzu, I.; Freunberger, S. A.; Wilkening, M. *Energy Environ. Sci.* **2014**, *7*, 2739−2752.

(30) Viswanathan, V.; Thygesen, K. S.; Hummelshoj, J. S.; Norskov, J. K.; Girishkumar, G.; McCloskey, B. D.; Luntz, A. C. *J. Chem. Phys.* **2011**, *135*, 214704.

(31) Varley, J. B.; Viswanathan, V.; Nørskov, J. K.; Luntz, A. C. *Energy Environ. Sci.* **2014**, *7*, 720−727.

(32) Knudsen, K. B.; Luntz, A. C.; Jensen, S. H.; Vegge, T.; Hjelm, J. *J. Phys. Chem. C* **2015**, *119*, 28292−28299.

(33) Luntz, A. C.; Viswanathan, V.; Voss, J.; Varley, J. B.; Nørskov, J. K.; Scheffler, R.; Speidel, A. *J. Phys. Chem. Lett.* **2013**, *4*, 3494−3499.

(34) Adams, B. D.; Black, R.; Williams, Z.; Fernandes, R.; Cuisinier, M.; Berg, E. J.; Novak, P.; Murphy, G. K.; Nazar, L. F. *Adv. Energy Mater.* **2015**, *5*, 1400867.

(35) Freunberger, S. A.; Chen, Y.; Drewett, N. E.; Hardwick, L. J.; Barde, F.; Bruce, P. G. *Angew. Chem., Int. Ed.* **2011**, *50*, 8609−13.

(36) Leskes, M.; Moore, A. J.; Goward, G. R.; Grey, C. P. *J. Phys. Chem. C* **2013**, *117*, 26929−26939.

(37) Black, R.; Oh, S. H.; Lee, J. H.; Yim, T.; Adams, B.; Nazar, L. F. *J. Am. Chem. Soc.* **2012**, *134*, 2902−5.

(38) Wen, R.; Hong, M.; Byon, H. R. *J. Am. Chem. Soc.* **2013**, *135*, 10870−6.

(39) Xia, C.; Waletzko, M.; Chen, L.; Peppler, K.; Klar, P. J.; Janek, J. *ACS Appl. Mater. Interfaces* **2014**, *6*, 12083−92.

(40) Black, R.; Lee, J. H.; Adams, B.; Mims, C. A.; Nazar, L. F. *Angew. Chem., Int. Ed.* **2013**, *52*, 392−6.

(41) Meini, S.; Tsiouvaras, N.; Schwenke, K. U.; Piana, M.; Beyer, H.; Lange, L.; Gasteiger, H. A. *Phys. Chem. Chem. Phys.* **2013**, *15*, 11478−93.

(42) Gowda, S. R.; Brunet, A.; Wallraff, G. M.; McCloskey, B. D. *J. Phys. Chem. Lett.* **2013**, *4*, 276−9.

(43) Ma, L.; Luo, X.; Kropf, A. J.; Wen, J.; Wang, X.; Lee, S.; Myers, D. J.; Miller, D.; Wu, T.; Lu, J.; Amine, K. *Nano Lett.* **2016**, *16*, 781−5.

(44) Park, J.-B.; Luo, X.; Lu, J.; Shin, C. D.; Yoon, C. S.; Amine, K.; Sun, Y.-K. *J. Phys. Chem. C* **2015**, *119*, 15036−15040.

(45) Lu, J.; Cheng, L.; Lau, K. C.; Tyo, E.; Luo, X.; Wen, J.; Miller, D.; Assary, R. S.; Wang, H. H.; Redfern, P.; Wu, H.; Park, J. B.; Sun, Y. K.; Vajda, S.; Amine, K.; Curtiss, L. A. *Nat. Commun.* **2014**, *5*, 4895.

(46) Xiao, J.; Mei, D.; Li, X.; Xu, W.; Wang, D.; Graff, G. L.; Bennett, W. D.; Nie, Z.; Saraf, L. V.; Aksay, I. A.; Liu, J.; Zhang, J. G. *Nano Lett.* **2011**, *11*, 5071−8.

(47) Chen, Y.; Freunberger, S. A.; Peng, Z.; Fontaine, O.; Bruce, P. G. *Nat. Chem.* **2013**, *5*, 489−494.

(48) Walker, W.; Giordani, V.; Bryantsev, V. S.; Uddin, J.; Zecevic, S.; Addison, D.; Chase, G. V. Toward Efficiently Rechargeable Li-O2 Batteries: Freely Diffusing Catalysts and O2 Electrode-Stable Solvents. In *PRiME 2012*; The Electrochemical Society: Honolulu, 2012; Vol. MA2012-02, p 1112.

(49) Lim, H. D.; Song, H.; Kim, J.; Gwon, H.; Bae, Y.; Park, K. Y.; Hong, J.; Kim, H.; Kim, T.; Kim, Y. H.; Lepro, X.; Ovalle-Robles, R.; Baughman, R. H.; Kang, K. *Angew. Chem., Int. Ed.* **2014**, *53*, 3926−31.

(50) Bergner, B. J.; Schürmann, A.; Peppler, K.; Garsuch, A.; Janek, J. *J. Am. Chem. Soc.* **2014**, *136*, 15054−15064.

(51) Matsuda, S.; Hashimoto, K.; Nakanishi, S. *J. Phys. Chem. C* **2014**, *118*, 18397−18400.

(52) Yang, L.; Frith, J. T.; Garcia-Araez, N.; Owen, J. R. *Chem. Commun.* **2015**, *51*, 1705−8.

(53) Lacey, M. J.; Frith, J. T.; Owen, J. R. *Electrochem. Commun.* **2013**, *26*, 74−76.

(54) Zhu, Y. G.; Jia, C.; Yang, J.; Pan, F.; Huang, Q.; Wang, Q. *Chem. Commun.* **2015**, *51*, 9451−4.

(55) Chase, G. V.; Zecevic, S.; Wesley, T. W.; Uddin, J.; Sasaki, K. A.; Vincent, P. G.; Bryantsev, V.; Blanco, M.; Addison, D. D. Soluble oxygen evolving catalysts for rechargeable metal-air batteries. U.S. Patent Appl. 13/093,759, 2012.

(56) Wu, F.; Lee, J. T.; Nitta, N.; Kim, H.; Borodin, O.; Yushin, G. *Adv. Mater.* **2015**, *27*, 101−108.

(57) Liu, T.; Leskes, M.; Yu, W.; Moore, A. J.; Zhou, L.; Bayley, P. M.; Kim, G.; Grey, C. P. *Science* **2015**, *350*, 530−533.

(58) Torres, W. R.; Herrera, S. E.; Tesio, A. Y.; Pozo, M. d.; Calvo, E. J. *Electrochim. Acta* **2015**, *182*, 1118−1123.

(59) Qiao, Y.; Ye, S. *J. Phys. Chem. C* **2016**, DOI: 10.1021/acs.jpcc.5b11692.

(60) Sun, D.; Shen, Y.; Zhang, W.; Yu, L.; Yi, Z.; Yin, W.; Wang, D.; Huang, Y.; Wang, J.; Wang, D.; Goodenough, J. B. *J. Am. Chem. Soc.* **2014**, *136*, 8941−6.

(61) Bergner, B. J.; Hofmann, C.; Schurmann, A.; Schroder, D.; Peppler, K.; Schreiner, P. R.; Janek, J. *Phys. Chem. Chem. Phys.* **2015**, *17*, 31769−79.

(62) Feng, N.; He, P.; Zhou, H. *ChemSusChem* **2015**, *8*, 600−602.

(63) Kundu, D.; Black, R.; Adams, B.; Nazar, L. F. *ACS Cent. Sci.* **2015**, *1*, 510−515.

(64) Behl, W. K. *J. Electrochem. Soc.* **1989**, *136*, 2305−2310.

(65) Zhang, L.; Zhang, Z.; Amine, K. Redox Shuttle Additives for Lithium-Ion Battery. In *Lithium Ion Batteries - New Developments*; Belharouak, I., Ed.; InTech: Rijeka, Croatia, 2012; Chapter 7.

(66) Kwak, W.-J.; Hirshberg, D.; Sharon, D.; Shin, H.-J.; Afri, M.; Park, J.-B.; Garsuch, A.; Chesneau, F. F.; Frimer, A. A.; Aurbach, D.; Sun, Y.-K. *J. Mater. Chem. A* **2015**, *3*, 8855−8864.

(67) Landa-Medrano, I.; Olivares-Marín, M.; Pinedo, R.; Ruiz de Larramendi, I.; Rojo, T.; Tonti, D. *Electrochem. Commun.* **2015**, *59*, 24−27.

(68) Kwak, W.-J.; Hirshberg, D.; Sharon, D.; Afri, M.; Frimer, A. A.; Jung, H.-G.; Aurbach, D.; Sun, Y.-K. *Energy Environ. Sci.* **2016**, DOI: 10.1039/c6ee00700g.

(69) Nasybulin, E.; Xu, W.; Engelhard, M. H.; Nie, Z.; Burton, S. D.; Cosimbescu, L.; Gross, M. E.; Zhang, J.-G. *J. Phys. Chem. C* **2013**, *117*, 2635−2645.

(70) Zhai, D.; Wang, H. H.; Yang, J.; Lau, K. C.; Li, K.; Amine, K.; Curtiss, L. A. *J. Am. Chem. Soc.* **2013**, *135*, 15364−72.

(71) Yang, J.; Zhai, D.; Wang, H. H.; Lau, K. C.; Schlueter, J. A.; Du, P.; Myers, D. J.; Sun, Y. K.; Curtiss, L. A.; Amine, K. *Phys. Chem. Chem. Phys.* **2013**, *15*, 3764−71.

(72) Zhai, D.; Lau, K. C.; Wang, H. H.; Wen, J.; Miller, D. J.; Lu, J.; Kang, F.; Li, B.; Yang, W.; Gao, J.; Indacochea, E.; Curtiss, L. A.; Amine, K. *Nano Lett.* **2015**, *15*, 1041−6.

(73) Zhai, D.; Wang, H. H.; Lau, K. C.; Gao, J.; Redfern, P. C.; Kang, F.; Li, B.; Indacochea, E.; Das, U.; Sun, H. H.; Sun, H. J.; Amine, K.; Curtiss, L. A. *J. Phys. Chem. Lett.* **2014**, *5*, 2705−10.

(74) Ganapathy, S.; Adams, B. D.; Stenou, G.; Anastasaki, M. S.; Goubitz, K.; Miao, X. F.; Nazar, L. F.; Wagemaker, M. *J. Am. Chem. Soc.* **2014**, *136*, 16335−44.

(75) McCloskey, B. D.; Scheffler, R.; Speidel, A.; Bethune, D. S.; Shelby, R. M.; Luntz, A. C. *J. Am. Chem. Soc.* **2011**, *133*, 18038−41.

(76) McCloskey, B. D.; Bethune, D. S.; Shelby, R. M.; Mori, T.; Scheffler, R.; Speidel, A.; Sherwood, M.; Luntz, A. C. *J. Phys. Chem. Lett.* **2012**, *3*, 3043−3047.

(77) Meini, S.; Solchenbach, S.; Piana, M.; Gasteiger, H. A. *J. Electrochem. Soc.* **2014**, *161*, A1306−A1314.

(78) Ma, S.; Wu, Y.; Wang, J.; Zhang, Y.; Zhang, Y.; Yan, X.; Wei, Y.; Liu, P.; Wang, J.; Jiang, K.; Fan, S.; Xu, Y.; Peng, Z. *Nano Lett.* **2015**, *15*, 8084−90.

(79) Hojberg, J.; McCloskey, B. D.; Hjelm, J.; Vegge, T.; Johansen, K.; Norby, P.; Luntz, A. C. *ACS Appl. Mater. Interfaces* **2015**, *7*, 4039−47.

(80) Adams, B. D.; Black, R.; Radtke, C.; Williams, Z.; Mehdi, B. L.; Browning, N. D.; Nazar, L. F. *ACS Nano* **2014**, *8*, 12483−12493.

(81) Garcia, J. M.; Horn, H. W.; Rice, J. E. *J. Phys. Chem. Lett.* **2015**, *6*, 1795−9.

(82) Tsiouvaras, N.; Meini, S.; Buchberger, I.; Gasteiger, H. A. *J. Electrochem. Soc.* **2013**, *160*, A471−A477.

(83) Kundu, D.; Black, R.; Berg, E. J.; Nazar, L. F. *Energy Environ. Sci.* **2015**, *8*, 1292−1298.

(84) Xie, J.; Yao, X.; Madden, I. P.; Jiang, D. E.; Chou, L. Y.; Tsung, C. K.; Wang, D. *J. Am. Chem. Soc.* **2014**, *136*, 8903−6.

(85) Hassoun, J.; Croce, F.; Armand, M.; Scrosati, B. *Angew. Chem., Int. Ed.* **2011**, *50*, 2999−3002.

(86) Shi, L.; Xu, A.; Zhao, T. S. *Phys. Chem. Chem. Phys.* **2015**, *17*, 29859−66.

(87) Lim, H.; Yilmaz, E.; Byon, H. R. *J. Phys. Chem. Lett.* **2012**, *3*, 3210−5.

(88) Kang, S.; Mo, Y.; Ong, S. P.; Ceder, G. *Chem. Mater.* **2013**, *25*, 3328−3336.

(89) Yang, G.; Wang, Y.; Ma, Y. *J. Phys. Chem. Lett.* **2014**, *5*, 2516−21.

(90) Lau, K. C.; Lu, J.; Luo, X.; Curtiss, L. A.; Amine, K. *ChemPlusChem* **2015**, *80*, 336−343.

(91) Kumar, N.; Radin, M. D.; Wood, B. C.; Ogitsu, T.; Siegel, D. J. *J. Phys. Chem. C* **2015**, *119*, 9050−9060.

(92) McCloskey, B. D.; Valery, A.; Luntz, A. C.; Gowda, S. R.; Wallraff, G. M.; Garcia, J. M.; Mori, T.; Krupp, L. E. *J. Phys. Chem. Lett.* **2013**, *4*, 2989−93.

(93) Chen, Y.; Freunberger, S. A.; Peng, Z.; Barde, F.; Bruce, P. G. *J. Am. Chem. Soc.* **2012**, *134*, 7952−7.

(94) Schwenke, K. U.; Metzger, M.; Restle, T.; Piana, M.; Gasteiger, H. A. *J. Electrochem. Soc.* **2015**, *162*, A573−A584.

(95) Freunberger, S. A.; Chen, Y.; Peng, Z.; Griffin, J. M.; Hardwick, L. J.; Barde, F.; Novak, P.; Bruce, P. G. *J. Am. Chem. Soc.* **2011**, *133*, 8040−7.

(96) Yang, S.; He, P.; Zhou, H. *Energy Environ. Sci.* **2016**, *9*, 1650−1654.

(97) Gallant, B. M.; Mitchell, R. R.; Kwabi, D. G.; Zhou, J.; Zuin, L.; Thompson, C. V.; Shao-Horn, Y. *J. Phys. Chem. C* **2012**, *116*, 20800−20805.

(98) Bryantsev, V. S.; Uddin, J.; Giordani, V.; Walker, W.; Addison, D.; Chase, G. V. *J. Electrochem. Soc.* **2013**, *160*, A160−A171.

(99) Khetan, A.; Pitsch, H.; Viswanathan, V. *J. Phys. Chem. Lett.* **2014**, *5*, 2419−24.

(100) Jeong, Y. S.; Park, J. B.; Jung, H. G.; Kim, J.; Luo, X.; Lu, J.; Curtiss, L.; Amine, K.; Sun, Y. K.; Scrosati, B.; Lee, Y. J. *Nano Lett.* **2015**, *15*, 4261−8.

(101) Conway, B. E.; Phillips, Y.; Qian, S. Y. *J. Chem. Soc., Faraday Trans.* **1995**, *91*, 283−293.

(102) White, R. E. *J. Electrochem. Soc.* **1983**, *130*, 1096.

(103) Harding, J. R.; Lu, Y. C.; Tsukada, Y.; Shao-Horn, Y. *Phys. Chem. Chem. Phys.* **2012**, *14*, 10540−6.